Fractal Stability Border in Plane Couette Flow

Armin Schmiegel and Bruno Eckhardt

Fachbereich Physik und Institut für Chemie und Biologie des Meeres, der C.v. Ossietzky Universität, Postfach 25 03, D-26111 Oldenburg, Germany

*and Fachbereich Physik der Philipps Universität Marburg, D-35032 Marburg, Germany**

(Received 5 March 1997)

We study the dynamics of localized perturbations in plane Couette flow with periodic lateral boundary conditions. For small Reynolds numbers and small amplitude of the initial state the perturbation decays on a viscous time scale $t \propto \mathrm{Re}$. For Reynolds number larger than about 200, chaotic transients appear with lifetimes longer than the viscous one. Depending on the type of the perturbation, isolated initial conditions with infinite lifetime appear for Reynolds numbers larger than about 270–305. In this third regime, the lifetime as a function of Reynolds number and amplitude is fractal. These results suggest that in the transition region the turbulent dynamics is characterized by a chaotic repeller rather than an attractor. [S0031-9007(97)04759-5]

PACS numbers: 47.20.Ft, 05.45.+b, 47.15.Fe, 47.53.+n

For a variety of simple flows linear stability theory predicts and experiments verify that the transition to turbulence proceeds by a sequence of instabilities at well defined critical values of the control parameter [1,2]. Prominent examples include a layer of fluid heated from below, flow between rotating cylinders, liquid jets, and stratified fluids. The transition to turbulence in pipe flow [3] or plane Couette flow [4,5] and to spiral turbulence in the flow between counter-rotating cylinders [6] does not fit this pattern. If the Reynolds number is sufficiently large, turbulent dynamics can occur, although the laminar profile is still stable. A formal linear stability analysis predicts either no instability (as in plane Couette flow [7]) or one for Reynolds numbers larger than the ones where experiments begin to show turbulent behavior (e.g., plane Poiseuille flow [8]). The nature of the transition is different from the cases with a linear instability. It depends on the size of the perturbation [9], shows very strong intermittency [10,11], and has no sharply defined stability border [3].

Such observations can be explained, if the bifurcations are subcritical, for then the new state extends to lower values of the Reynolds number and can be reached starting from finite amplitude perturbations [12,13]. Simple models, based on interacting wave vector triads or truncations of Galerkin systems, are compatible with this view. However, it has not been possible to follow these upper branches all the way down to where they disappear and to identify a critical Reynolds number [14].

A different approach has recently focused on the eigenvectors of the linearized problem [15–18]. Very often the linearized hydrodynamic eigenvalue problem is not Hermitian, so that the eigenvectors are not orthogonal. As a consequence, small perturbations can be amplified a lot even if all eigenvalues are negative, and the neglect of nonlinear interactions can no longer be justified. This explains how in the absence of linear instability the stability region around the laminar profile becomes small, perhaps irrelevantly small. One can imagine that because of this growth some of the turbulence seen in these systems is noise induced [18].

To shed some more light on the dynamics in these cases we have studied the evolution of perturbations in a numerical model for plane Couette flow. The numerical method was designed specifically to allow accurate long integration times. The lifetime of these perturbations was mapped out in an amplitude–Reynolds number plane. This allowed us to identify three dynamical regimes and to study the transitions between them. The results indicate that there is no sharp transition to turbulence: the landscape of lifetimes has fractal features, with some isolated lifetimes longer than the finite integration time. Thus, whether an initial condition leads to an evolution identified as turbulent depends in a sensitive way on initial amplitude, Reynolds number, and the experimental observation time. This is in qualitative agreement with experiments on plane Couette flow [4,5] and consistent with observations on pipe flow [3]. In addition, the numerical results suggest that the turbulent state belongs to a transient repeller rather than a turbulent attractor [19,20].

The numerical model (see [21] for more details) is based on an expansion of the velocity field in Fourier and Legendre polynomials,

$$\mathbf{u}(x,y,z,t) = \sum_{\mathbf{k},p} \tilde{\mathbf{u}}_{\mathbf{k},p}(t) e^{i(k_x x + k_y y)} L_p(z) . \qquad (1)$$

The advantage of Legendre polynomials compared to Chebyshev polynomials is that they give rise to evolution equations which are energy conserving in the Eulerian, undriven limit, which is important for the long time evolution we want to study. For every velocity-component, we used a set of 37 Fourier modes on a hexagonal grid and 16 Legendre polynomials. The boundary conditions $\mathbf{u}(x,y,\pm H/2) = 0$ and continuity equation are included

 0031-9007/97/79(26)/5250(4)$10.00

within the Lagrange formalism of the first kind [21]. These restrictions finally leave 962 dynamically active degrees of freedom.

The basic flow is normalized to have velocity $\pm U_0$ at $z = \pm H/2$. The Reynolds number is defined as $\mathrm{Re} = U_0 H/2\nu$, with ν the kinematic viscosity. Lengths are measured in units of $H/2$ and time in units of $\tau = H/2U_0$. The Navier-Stokes equation for a perturbation $\mathbf{u}$ of the initial profile $\mathbf{U}_0 = U_0 z \mathbf{e}_x$,

$$\dot{\mathbf{u}} = -(\mathbf{u}\cdot\nabla)\mathbf{U}_0 - (\mathbf{U}_0\cdot\nabla)\mathbf{u} - (\mathbf{u}\cdot\nabla)\mathbf{u} - \frac{1}{\rho}\nabla p + \frac{1}{\mathrm{Re}}\Delta\mathbf{u} \qquad (2)$$

$$\nabla\cdot\mathbf{u} = 0\,, \qquad (3)$$

are replaced by nonlinear ordinary differential equations for the amplitudes $\tilde{\mathbf{u}}_{\mathbf{k},p}$. We verified that in the energy conserving limit integration errors remained small for scaled times up to 10 000. For $H = 1$ cm, the viscosity of water, and a Reynolds number of $\mathrm{Re} = 400$, this corresponds to about 10 min. In experiments a localized initial disturbance spreads and reaches the span wise walls within less than a minute [22,23]. The numerical calculations thus extend to a time region where in experiments the influence of the lateral walls is no longer negligible.

The initial state for our simulations was taken to be a poloidal vortex ring in the y-z plane,

$$\mathbf{u} = A\,\mathrm{curl}\,\mathrm{curl}\,\delta(x,y)e^{-10z^2}\,\mathbf{e}_x\,, \qquad (4)$$

with a variable amplitude A. We approximate the δ function by setting all real Fourier modes equal to one. As shown schematically in Fig. 1, the axis of the ring points in the $\mathbf{e}_x$ direction. To remove excess energy for large modes we integrated this state for five time units at $\mathrm{Re} = 400$ and used the resulting physically realistic initial condition in the subsequent studies. By this time the vortex ring is rotated into the x-y plane and is similar to the one induced by the vertical water jets in the experiments [4,22,24].

Three different flow regimes are distinguishable by their time series as shown in Fig. 2. For low Reynolds number, the energy of the perturbation decays smoothly, with a bump related to the non-normality of the linearized equations of motion. The time when this maximum is reached is in agreement with the estimate $t_{\max} \propto 0.117\mathrm{Re}$ in [25]. This is the first regime, dominated by the linearized equations.

Around $\mathrm{Re} = 300$ states show a qualitatively similar decay but only after an intermediate period of irregular dynamics. A lifetime can be defined by monitoring the z component of the velocity until it decays below a certain threshold. Below this threshold the perturbation decays as described by the linearized equations. In this second flow regime the lifetimes for perturbations are longer than estimated from the linearized equations. But one notes from Fig. 2 that the lifetime of the disturbance is not a monotonous function of Re: The evolution at $\mathrm{Re} = 400$ shows more fluctuations and violent bursts but its lifetime is shorter than at $\mathrm{Re} = 300$. In this third region, characterized by a nonmonotonic variation of lifetimes with amplitude and Reynolds number, some initial conditions do not decay within the numerical integration time. The signals for the decaying and nondecaying states are dynamically similar in the fluctuating states, and there is no precursor that indicates the decay of the perturbation.

The nonmonotonic variations of lifetime with Reynolds number and amplitude occur for Re above about 350 and cover an increasing range in amplitude. On a global scale (Fig. 3), one notes a rather rugged landscape with a few peaks reaching the maximal lifetimes followed in the numerical calculations. Because of the finite observation times in experiments, states are classified as decaying or turbulent when their lifetimes are below or above a certain threshold. A cut through the lifetime landscape shows isolated turbulent disturbances in the decaying region and isolated decaying disturbances in the turbulent region. Such a behavior has been seen in experiments on constant mass flow through a pipe [3]. The nonmonotonicity

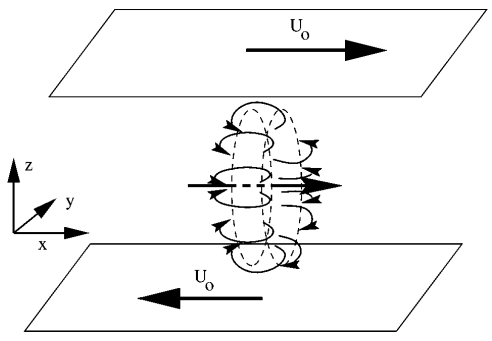

FIG. 1. Sketch of the flow geometry and the initial conditions for the perturbation. The poloidal vortex ring [Eq. (4)] has been enlarged for better visibility.

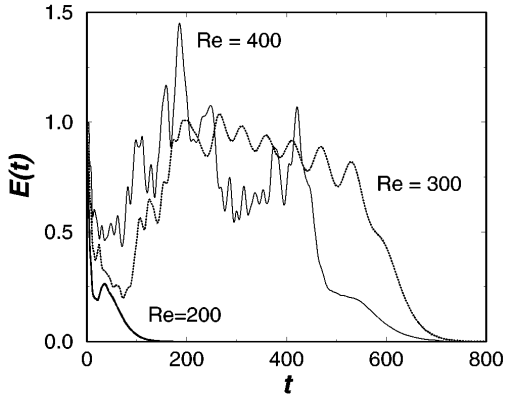

FIG. 2. Evolution of the energy in the perturbation vs time for three values of the Reynolds number.

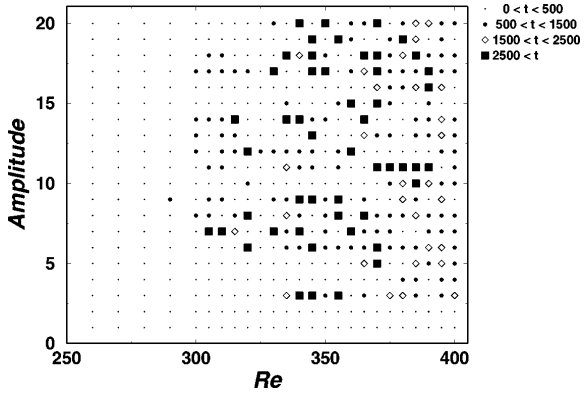

FIG. 3. Lifetime of perturbations as a function of Reynolds number Re and amplitude of the initial state. The lifetimes are grouped in intervals and shown by different symbols as indicated. The small dots with short lifetimes show the grid of initial conditions tested. The full squares indicate lifetimes above 2500 in scaled units. The integration was stopped at a scaled time of 3000.

observed there may thus be of dynamical origin and not due to experimental limitations.

The distribution of lifetimes as a function of amplitude and Reynolds number has fractal features. Magnification of successive intervals in amplitude (Fig. 4) for fixed Reynolds number or of intervals in Re for fixed amplitude reveals a self-similar pattern of lifetimes, without any obvious simplifications on smaller scales. The set of long lifetimes is reminiscent of the Cantor set one constructs by deleting subsets from intervals, where here the fraction deleted varies from level to level. The magnifications are reminiscent of lifetime pictures obtained in chaotic scattering [26–28]. This analogy suggests that the long

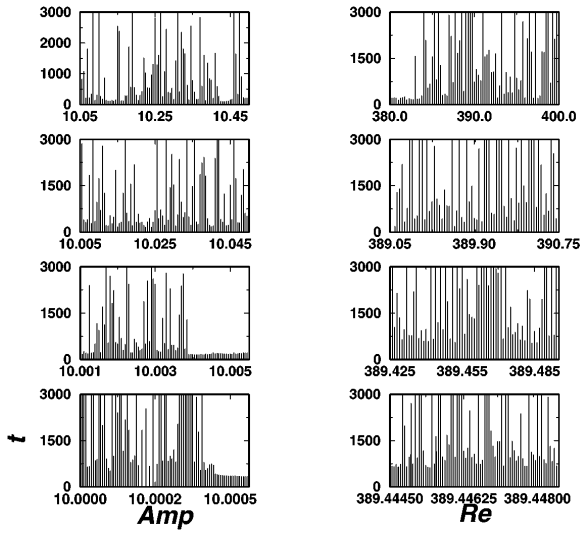

FIG. 4. Successive magnifications of cuts through the lifetime landscape of Fig. 3, for Re = 380 and varying amplitude (left column) and for fixed amplitude $A = 10$ and varying Reynolds number (right column).

lifetimes arise for initial perturbations which are close to the stable manifold of a strange repeller in phase space. Then arbitrarily large lifetimes should be possible and the "turbulent" state would be supported by a repeller rather than an attractor.

As the Reynolds number increases the number of long lived disturbances increases and they cover an ever increasing region in phase space and extend to smaller amplitudes. Phase space becomes more densely filled with the stable and unstable manifolds of the saddles so that trajectories trapped in this tangle need more and more time before they can escape and relax to the laminar profile. This is in line with previous observations in large systems [19] and pipe flow [29] that long lived transients can imitate a permanent turbulent state. Clearly, a measure of the thickness of the repeller or an estimate of the lifetime of transients as a function of Reynolds number would be highly desirable but is presently beyond our numerical or analytical abilities.

Further support for these observations is derived from a low dimensional system of ordinary differential equations for a shear flow where we can follow the dynamics more efficiently and can also study the nature of the repeller in more detail [30]. In particular, we find that in a saddle node bifurcation new stationary states are born which, however, are all unstable. The stable and unstable manifolds of these saddles do not meet smoothly and presumably create a strange repelling set. The dimension of this repelling set is rather high. A determination of its dimension by the usual methods is made difficult by the fact that the dimension is high and the time a typical trajectory spends on the repeller is much too short. However, an indication of its dimension is given by the number of unstable eigenvalues of the local linearization. In our simulation of plane Couette flow at Re = 400 the number of positive eigenvalues varied between 30 and 80. The maximum eigenvalue of the local linearization was about 0.35 in inverse time units.

As mentioned, the repeller presumably forms around the hyperbolic tangle of the stable and unstable manifolds of stationary states. Candidates for such stationary states in plane Couette flow are the states found previously by Nagata [31] and Clever and Busse [32,33]. These states appear for Reynolds numbers above about 125. For larger Reynolds numbers we have found further states, in accord with the observations on the model. But there remains a discrepancy between the Reynolds number for the occurrence of stationary states (about 125) and the initiation of turbulence around Re $\sim$ 300. This might be connected to the dependence on the other parameters in the model, and to the choice of initial conditions. In our model, the saddle node bifurcation occurs for Re $\approx$ 267, rather close to the first long lived initial condition for rings oriented along the $\mathbf{e}_y$ axis. However, for rings along the $\mathbf{e}_x$ axis, the transition occurs only for Re $>$ 305. This strong dependence on initial conditions points to a strong

anisotropy of the distribution of stable manifolds in phase space. Numerical experiments to analyze this further are in progress.

This scenario may be relevant for other shear flows without linear instability and, perhaps, for some systems with a subcritical transition.

*Permanent address.

[1] S. Chandrasekhar, *Hydrodynamic and Hydromagnetic Stability* (Oxford University Press, Oxford, 1961).
[2] P. G. Drazin and W. H. Reid, *Hydrodynamic Stability* (Cambridge University Press, Cambridge, 1981).
[3] A. G. Darbyshire and T. Mullin, J. Fluid Mech. **289**, 83–114 (1995).
[4] F. Daviaud, J. Hegseth, and P. Bergé, Phys. Rev. Lett. **69**, 2511–2514 (1992).
[5] O. Dauchot and F. Daviaud, Europhys. Lett. **28**, 225–230 (1994).
[6] D. Coles, J. Fluid Mech. **21**, 385–425 (1965).
[7] V. A. Romanov, Funkt. Anal. Appl. **7**, 137 (1973).
[8] S. A. Orszag and L. C. Kells, J. Fluid Mech. **96**, 159–205 (1980).
[9] D. J. Acheson, *Elementary Fluid Mechanics* (Oxford University Press, Oxford, 1990).
[10] J. Zang, D. Stassinopoulos, P. Alstroem, and M. T. Levinsen, Phys. Fluids **5**, 1722–1726 (1994).
[11] D. Stassinopoulos, J. Zang, P. Alstroem, and M. T. Levinsen, Phys. Rev. E **59**, 1189–1193 (1994).
[12] J. T. Stuart, J. Fluid. Mech. **9**, 353–370 (1960).
[13] J. Watson, J. Fluid. Mech. **9**, 371–389 (1960).
[14] A. Rauh, T. Zachrau, and J. Zoller, Physica (Amsterdam) **86D**, 603–620 (1995).
[15] L. Boberg and U. Brosa, Z. Naturforsch. A **43**, 697–726 (1988).
[16] L. N. Trefethen, A. E. Trefethen, S. C. Reddy, and T. A. Driscoll, Science **261**, 578–584 (1993).
[17] T. Gebhardt and S. Grossmann, Phys. Rev. E **50**, 3705–3711 (1994).
[18] B. F. Farrell and P. J. Ioannou, Phys. Rev. Lett. **72**, 1188–1191 (1994).
[19] J. P. Crutchfield and K. Kaneko, Phys. Rev. Lett. **60**, 2715–2718 (1988).
[20] U. Brosa, J. Stat. Phys. **55**, 1303–1312 (1989).
[21] A. Schmiegel and B. Eckhardt (to be published).
[22] N. Tillmark and P. H. Alfredsson, J. Fluid Mech. **235**, 89–102 (1992).
[23] N. Tillmark, Europhys. Lett. **32**, 481–485 (1995).
[24] S. Malerud, K. J. Måløy, and W. I. Goldburg, Phys. Fluids **7**, 1949–1955 (1995).
[25] S. C. Reddy and D. S. Henningson, J. Fluid. Mech. **252**, 209–238 (1993).
[26] B. Eckhardt and H. Aref, Philos. Trans. R. Soc. London A **326**, 655–696 (1988).
[27] B. Eckhardt, Physica (Amsterdam) **33D**, 89–98 (1988).
[28] E. Ott, *Chaos in Dynamical Systems* (Cambridge University Press, Cambridge, 1993).
[29] U. Brosa, Z. Naturforsch. A **41**, 1141–1153 (1986).
[30] B. Eckhardt and A. Mersmann (to be published).
[31] M. Nagata, J. Fluid Mech. **217**, 519–527 (1990).
[32] R. M. Clever and F. H. Busse, J. Fluid Mech. **234**, 511–527 (1992).
[33] R. M. Clever and F. H. Busse, in *Waves and Nonlinear Processes in Hydrodynamics*, edited by J. Grue *et al.*, (Kluwer Academic Publishers, Amsterdam, 1996), pp. 209–226; R. M. Clever and F. H. Busse, J. Fluid Mech. **344**, 137 (1997).